THE JOURNAL OF PHYSICAL CHEMISTRY C

Article

Inorganic Aromaticity of Mn-Ring Cluster in Layered Li(NiMn)O

Zongxiang Hu, Jiaxin Zheng, Chao Xin, Gaofeng Teng, Yunxing Zuo, and Feng Pan

J. Phys. Chem. C, **Just Accepted Manuscript** • DOI: 10.1021/acs.jpcc.7b10968 • Publication Date (Web): 31 Jan 2018

Inorganic Aromaticity of Mn_6-Ring Cluster in Layered $Li(Ni_{0.5}Mn_{0.5})O_2$

Zongxiang Hu[†], Jiaxin Zheng[†], Chao Xin[†], Gaofeng Teng, Yunxing Zuo, and Feng Pan*

School of Advanced Materials, Peking University, Shenzhen Graduate School, Shenzhen 518055, People's Republic of China.

[†]These authors contributed equally to this work.

*Corresponding author: panfeng@pkusz.edu.cn

ABSTRACT: Using ab initio calculations, here we identified an inorganic aromaticity of Mn_6-ring cluster in layered $Li(Ni_{0.5}Mn_{0.5})O_2$ with Ni/Li mixing. The comparison between delocalized orbitals Mn-d_{z2} in Mn_6-ring and benzene-p_z uncovers the fundamental similarity between a local cluster and benzene in electronic behavior. We also demonstrate that the delocalized interactions between transition metals (TMs) play a great role on forming the inorganic aromaticity of Mn_6-ring in the layered TM $Li(Ni_{0.5}Mn_{0.5})O_2$ (with Ni/Li mixing) via a two-level hierarchy: (i) the same TM ions (here manganese) can interact with each other directly through delocalized orbitals Mn-*d* in Mn_6-ring, and the local symmetry can impose restrictions on this delocalization. The direct exchange interactions play an important role at this level; (ii) the anions, here oxygen, can match with these delocalized orbitals of *d*-manifold via bridged bonds to share their electrons with TM ions to create the superexchange interactions, which enable forming solid local cluster Mn_6O_{24}. The present findings

broaden our knowledge about the interactions between transition metals and provide important factors on governing the local ordering in TM compounds.

Introduction

Since the first introduction of aromaticity on the structure of benzene by Kekule´'s,[1] it has become one of the fascinating topics in chemistry, attracting continuous interests both for experimentalists and theoreticians over a century.[2-6] Although aromaticity is still a rather fuzzy concept, it is generally agreed that aromatic compounds are planar, cyclic, fully conjugated systems which possess delocalized π-electrons. This cyclically delocalized and conjugate electronic structure confers special properties of aromatic compounds, including ring bond lengths which are intermediate between normal single and double bonds, diamagnetic ring currents (diatropicity), and high thermodynamic stability.[2] Interestingly, besides the benzene and its heterocyclic analogues (a CH group of benzene is formally replaced by an isoelectronic heteroatom, include pyridine, phosphabenzene, arsabenzene, pyrylium, thiabenzene, and even a transition metal and its associated ligands), aromatic metallic rings have also been observed in gas phases, such as $[M_2(GaH)_3]$ (M) Li, Na, K),[7] Al_4^-,[8] XAl_3^- (X = Si, Ge, Sn, Pb),[9] and Pn_5^- (Pn = P, As, Sb, Bi).[10] Furthermore, the first aromatic all-metal heterocycle, $[ZnBi_4]^{3-}$, was found in the metallic salt, K_6ZnBi_5, has been synthesized and structurally characterized.[11]

Both previous experimental and theoretical investigations on the multiple-cation ordering/disordering in layered transition metal (TM) oxides, which is a widely used

cathode materials for rechargeable lithium-ion batteries, demonstrated that the arrangement of cations does not employ a random configuration but an ordering pattern.[12-18] For examples, using high-resolution solid-state NMR, synchrotron X-ray diffraction, electron diffraction and neutron diffraction studies, it is suggested that short-range in-plane ordering is almost universal in mixed transition-metal (NMC) layered oxides.[12-13, 16] Combined with first principles simulations, a well-characterized $2\sqrt{3}$-type structure model in $Li(Ni_{0.5}Mn_{0.5})O_2$ (without cobalt) with 8.7% Li/Ni exchange has been established: six manganese ions preferentially occupy a coordination ring (Mn_6) surrounding the central Li-ion in the transition-metal layers, while twelve nickel ions tend to form the outer ring encircling the first-ring.[13-14] This unique local coordination environment looks like a flower-ordering with surprising six-fold symmetry and all the local coordination environments could come into being an organized periodical structure. Subsequently, they found that the flower-like structure transforms from the ground state zigzag-ordered structure without Li/Ni disorder undergoing a phase transition over 550°.[19] Thus, concerns have been raised: does the Mn_6 ring in $Li(Ni_{0.5}Mn_{0.5})O_2$ show similar aromaticity as the C_6 ring in benzene both? If it is, what's the origin to form the inorganic aromaticity for Mn_6 ring in layered $Li(Ni_{0.5}Mn_{0.5})O_2$?

Herein, using ab initio calculations, we investigate the electronic structure and physicochemical origin of local Mn_6 ring in layered $Li(Ni_{0.5}Mn_{0.5})O_2$. By carefully surveying the symmetry and electronic structure of local units (Mn_6) in $Li(Ni_{0.5}Mn_{0.5})O_2$, it is found that such holistic *d*-electron behavior of Mn_6O_{24} cluster is

indeed similar to the delocalized carbon-p_z (C-p_z) in benzene. Analogously, the delocalized interactions between metals contribute to local cation ordering and aromaticity of Mn_6-ring with six-fold symmetry in $Li(Ni_{0.5}Mn_{0.5})O_2$. We also found that a delocalized mechanism can promote the formation of Mn_6 ring via a two-level hierarchy of interaction: (i) the same TM ions (here manganese) can interact with each other directly through delocalized orbitals Mn-d_{z2} in Mn_6 ring, and the local symmetry can impose restrictions on this delocalization. The direct exchange interactions play an important role at this level; (ii) the anions, here oxygen, can match with these delocalized orbitals of *d*-manifold via bridged bonds to share their electrons with TM ions to create the superexchange interactions, which enable forming solid local cluster Mn_6O_{24}. It also should be noted that if there is no Li/Ni exchange, Ni centered in the clusters can weaken Mn-O bonding and jeopardize the existence of the clusters.

Results & Discussion

Aromaticity in structure characteristic. According to previous studies, the most energetic favorable configurations, flower-like and zig-zag structures, are taken into account in $Li(Ni_{0.5}Mn_{0.5})O_2$.[13, 20] All structures $Li(Ni_{0.5}Mn_{0.5})O_2$ built in this work are layered structures with space group $R\bar{3}m$, as the α-$NaFeO_2$ model. Figure 1 shows the supercells (Figure 1a and 1b) and corresponding in-plane arrangements (Figure 1c and 1d). There are three layers of TM, and three layers of Li-ions in each supercell. Stacking sequences of in-plane ordering perpendicular to the layers of these supercells adopts a stacking sequence of *abcabc*...along the $\boldsymbol{c}_{hex.}$ axis. For flower-like structure,

the in-plane dimension with 8.7% Li/Ni exchange possesses a $2\sqrt{3}\boldsymbol{a}_{hex.} \times 2\sqrt{3}\boldsymbol{a}_{hex.}$ ordering. The supercells contain twenty-four and thirty-six formula units of $Li(Ni_{0.5}Mn_{0.5})O_2$ for zig-zag and flower-like ordering structures, respectively. All calculations were performed by GGA+U method which integrates the GGA with an on-site Coulomb potential for the *d*-electronics.[21] The values for the Hubbard-U parameters for Ni and Mn were determined from previous computational work.[15] We employed the reported effective U values 5.96 eV and 5.10 eV for Ni ions and Mn ions, respectively. For reason that the values of U are system dependent and can affect results of electronic structures, we also performed hybrid functional calculation to verify reliability of electronic structure obtained by GGA+U calculations. The results obtained by HSE06 calculation are in accordance with our GGA+U results (See detailed discussion in Supplement of computational methods in Supporting Information). The calculated lattice parameters of these supercells with different magnetic configurations and the corresponding magnetic moments are consistent with previous calculations and close to experimental data (Table S1).[20] The Figure S1 shows the magnetic configurations applied tore calculation. The energies of zig-zag, flower-like structure with different magnetic configurations are shown in Table S2. It can be seen that for all atomic structures, the ferrimagnetic configurations are energy favorable. The absence of Jahn-Teller active Mn^{3+} and Ni^{3+} is in accordance with the calculated magnetic moments.[22] By comparing the energy of zig-zag and flower-like structures, we find the energy of zig-zag structure is lower than that of flower-like structure, which is consistent with previous calculations.[13] The zigzag-like state with

no Li/Ni exchange (-23.05951 eV/F.U.) is energetic favorable than flower-like state (-23.03169 eV/F.U.), indicating more stable at low temperature. However, after taking 8.3% Li/Ni mixing into consideration, it is revealed that the energy of zig-zag structure with identical Li/Ni mixing is higher than the energy of flower-like structure. Thus, when Li/Ni exchange occurs, the flower-like structure is more energetic favorable (12.8 meV/F.U.) than zig-zag structure, so the zig-zag configuration would undergo phase transition and transform to the more stable flower-like configuration with increasing temperature. The results are in accordance with previous theoretical works by DFT calculations and Monte Carlo simulations.[13, 19]

Figure 2a and 2b show hypothetic clusters (h-cluster) extracted from flower-like and zig-zag structures, respectively. For the flower-like configuration with Li/Ni mixing, there are six-Mn (Mn_6) rings with one Li in the center in Mn_6O_{24} h-cluster coordinated by O groups, whereas there are Mn-chains in zig-zag structures. According to O local environments (or lengths of Mn-O bonds), the O in Mn_6O_{24} h-cluster can be divided into three groups: O^f_1 (connect with two Mn and one Li), O^f_2 (connect with two Mn and one Ni), and O^f_3 (connect with one Mn and two Ni) as shown in Figure 2a and Figure S2a. The lengths of Mn-O bonds are nearly identical in the same group but different in the three groups, with 1.980, 1.958, and 1.921 Å, respectively. The outmost O^f_3 ring of Mn_6O_{24} shows the shortest bonds, indicating that there is a real cluster shrinking as a whole to improve the stability. We then calculated the electron localization function (ELF) of the flower-like configuration (Figure S3) and found that Mn_6O_{24} h-cluster can be viewed as six Mn coordinated by these three

O groups. By contrast, there are only two environments for O in the zig-zag structure (connect with two Mn and one or two Ni), as shown in Figure 2b and Figure S2b. The O^z_2 linked to two Ni have shorter Mn-O bonds (1.925 Å), the same as O^f_3 in flower-like structure. The Mn-O^z_1 bonding to two Mn have unequal lengths of bonds, with lengths of 1.953 and 1.987 Å, respectively, arranged alternately along the Mn-O zig-zag chain. The distances of six Mn-Mn bonds in Mn_6O_{24} cluster of the flower-like structure are about 2.898 Å (which would be distorted 2.937 Å when there is near the upper and lower antisite-Ni, See detailed discussion in Section S3 in Supporting Information), which are shorter than that in zigzag structures (2.946 Å) to show a more compact tendency, which is analogous to six carbon-carbon (C-C) bonds in benzene with congruent length (1.40 Å) to be shorter than a single bond (1.47 Å) but greater than a double bond (1.35 Å). This intermediate bond length is consistent with electron delocalization: the electrons for C–C bonding are distributed equally between each of the six carbon atoms. Thus, form structure analogous, Mn_6-ring in flower-like structure is similar to C_6-ring in benzene with aromaticity in structure characteristic, whereas Mn-chain in zig-zag structure for is similar to C-chain of olefin and alkane in organic chemistry.

Aromaticity in electronic behavior. Electronic structures of Mn_6-ring of Mn_6O_{24} cluster in flower structure and Mn-Mn bonds in zig-zag configuration are further analyzed. The projected density of states (PDOS) of the Mn majority-spin *d* states of the two h-clusters is shown in Fig. 2c and Fig. 2d, respectively. From the PDOS of Mn_6-ring, it can be seen that the d_{yz} states overlap with the d_{xz} states in the whole

energy range, and meanwhile the d_{xy} states and d_{x2-y2} states also superpose mutually through total energy interval, letting d_{z2} states alone. The d states overlapping with each other are degenerate:

$$\begin{cases} d_{z2}; \\ d_{xz}, d_{yz}; \\ d_{x2-y2}, d_{xy}. \end{cases}$$

We further checked the PDOS of individual Mn in Mn_6-ring (Figure 2e): the PDOS of individual Mn shows evident distinctions lacking degeneracies of d states that Mn_6-ring as a whole has. This suggests that the degeneracy is inseparable nature of whole for Mn_6-ring due to entanglements between Mn cations. By contrast, from the PDOS of Mn-chain in zigzag structure (Figure 2d), it is found that its Mn-d states don't show high degeneracy compared with the flower-like structure. In addition, the congruence between PDOS of individual Mn and all Mn of Mn-chain in for the zig-zag configuration further demonstrates that total behaviors of Mn cations of Mn-chain are merely linear additivity of individual Mn cation (Figure 2f), showing an obvious difference from the Mn_6-ring in flower-like configuration. In other words, Mn cations of Mn-chain in the zig-zag chain are comparatively isolated. A classical organic chemical picture of benzene and olefin might help us to understand the difference between Mn_6-ring and Mn-chain: with same surplus C-p_z electrons, but closed high-symmetry C_6 enables more effective C-p_z delocalization than open low-symmetry C-chain. Similarly to organic aromaticity, Mn_6-ring also shows more delocalized d states to create conjugate π-electrons than that of Mn-chain due to the closed and high-symmetry system.

Ordinarily, we next estimate the degeneracy of energy level of Mn_6-ring through

the symmetry directly and strictly. The symmetry of Mn_6O_{24} h-cluster belongs to point group D_{3d}, and the schematic diagram for Mn_6O_{24} cluster is sketched with symmetry operations of point group D_{3d} explicitly (Figure S4). Decomposition of the *d* states according to group D_{3d} are shown in Table S3,[23] which can help us straightforward estimate energy division of *d* states of a free atom interacted to electrostatic potential with D_{3d} symmetry. From the first column of Table S3, we can immediately get that orbitals d_{yz} and d_{xz} (also for d_{xy} and d_{x2-y2}) have the same energy distributions, labeled with two-fold E_g representation, while d_{z2} belongs to nondegenerate state labeled with A_{1g} representation. Interestingly, *d* states of Mn_6-ring also decompose to A_{1g} (d_{z2}) and E_g (d_{yz}, d_{xz}; d_{xy}, d_{x2-y2}) groups just like one integral "atom". Obviously, the behaviors of *d* states originate from Mn_6-ring serve as a whole, where six Mn intangle with each other.

The degeneracy of *d*-states of Mn_6-ring demonstrates the existence of a direct interaction between six Mn. Benzene is the typical representative of direct delocalized interaction. The six C-p_z orbitals in C_6 can interact with each other and produce new orbital assignments restricted by the D_{6h} symmetry of the C_6H_6 molecule. The energy levels and wavefunctions of delocalized C-p_z in benzene are shown in Figure 3a and 3b. The reassigned six orbitals are two nondegenerate states a_{2u}, b_{2g}, and two doublet states e_{1g}, e_{2u}. Each of these reassigned orbitals is contributed by part of original six C-p_z orbitals actually. In parallel, the hybridization between Mn *d*-orbitals also changes energies of original *d*-orbitals and generates new delocalized orbitals. We take A_{1g} (d_{z2}) as an example to visualize specific forms of these delocalized orbitals.

Figure 3c shows the PDOS of d_{z2} states of Mn_6-ring. It can be seen that the hybridization of six d_{z2} orbitals of Mn_6-ring can produce a_{1g}, e_u, e_g and a_{1u} delocalized orbitals from left to right in energy. So the one-to-one corresponding relations between Mn-d_{z2} and C-p_z can be built (Figure 3b and 3d). In energy intervals -5.5 ~ -4.0 eV and -3.5 ~ -2.0 eV, the doublet states e_u and e_g are split (Figure 3c) because of the distortion of Mn_6O_{24} cluster with the influence of antisite-Ni (See detailed discussion in Section S3 in Supporting Information). The direct hybridization of E_g group, (d_{yz}, d_{xz}) and (d_{xy}, d_{x2-y2}), is examined furthermore (Figure S5), in which doublet states e_u and e_g are also split. It should be noted that the energy levels are broadened by crystal periodic potential and different energy levels are not equally distributed. Although delocalization in Mn_6-ring is not exactly the same way as in organic chemistry, aromaticity with conjugate π-electron delocalization based on the direct interaction in Mn_6-ring in Mn_6O_{24} and C_6-ring of benzene is similar.

Forming of d-pπ bonding enabling aromaticity of Mn_6-ring. Noticing the stronger overlapping between delocalized Mn_6-ring and O-*p* orbitals in Mn_6O_{24} cluster (Figure S3), to detail the interaction between *d* orbitals of Mn_6-ring and O-*p* orbitals, we calculate the partial charge density (PCD) ranged in different energy intervals (Figure 4a). Interestingly, a particular bonding form can be seen in the PCD pictures for Mn-O^f_1 and Mn-O^f_2 bonds. The shape is similar to a bridge linking two adjacent Mn equally, which forms an effective (*d-p-d)π* bonding. The distribution of this bonding is quite broad in energy. Figure 4b and 4c show the schematic diagram of (*d-p-d)π* bonding between delocalized Mn_6-ring and O groups. First, we take d_{z2} orbitals to

exemplify bonding process (Figure 4b). Obviously, to form this bonding, the dumbbell-shaped *p* orbitals of O^f_1 and O^f_2 should parallel two adjacent Mn. However, the two terminals of dumbbell are one positive and one negative, respectively, and the localized d_{z2} orbitals can not form this (*d-p-d*)π bonding because negative terminal of *p* orbital always counteracts with positive *d* states (left part in Figure 4b). But for reassigned orbitals of Mn in Mn_6-ring like a_{1u} (the right part in Figure 4b), wavefunctions of adjacent Mn d_{z2} states are opposite sign and exactly match to two terminals of *p* orbital bonding to two Mn equally. Figure 4c shows d_{x2-y2} orbitals form this (*d-p-d*)π bonding. The existence of (*d-p-d*)π bonding in broad energy range is also due to the delocalized *d* states in broad energy range. At the position of peaks a_{1g} (below energy -7.0 eV), we can not find (*d-p-d*)π bonding, because localized *d* states have a_{1g} symmetry. When we look into Mn-O^f_3 bonds, familiar images come to our minds, and that is the shape of sigma-bond ordinarily symmetrized with respect to rotation about the bond axis. As we know, the sigma-bond is the strongest bond, which explains why the outmost Mn-O^f_3 bonds are the shortest. So Mn_6-ring can bond to O tightly through delocalized *d* states to generate "big conjugate (*d-p-d*)π-electron delocalization". We call this property of consolidating stability "aromaticity" to some extent.

The origin of aromaticity of Mn_6-ring. Electron spin coupling has been raised to describe an aromatic characteristic of benzene: the p_z in benzene are certainly localized but aromaticity of this system arises from the symmetry coupling of electron spins around the carbon framework.[24] The reason why Mn-*d* states can delocalize

with each other can be understood from the magnetic direct interaction between magnetic shells with electron spin coupling.[25] The *d* electrons can usually be delocalized in metals but localized in metallic oxides. Figure S6 shows the form of *d*-orbital division and electronic configuration of individual Mn^{4+} and Ni^{2+} octahedrally coordinated by six O. It can be seen that the e'_g orbitals spread toward ligand directly from the plots of e'_g orbitals, so their delocalizability usually have been isolated by O. In TM layers, the MO_6 (M = Mn or Ni) octahedra share edges, and itinerant electrons in the t'_{2g} orbitals straightforward spread to each other, making direct electronic exchange possible.[25] Thus, the delocalization is strengthened through magnetic exchange between half-filling t'_{2g} orbitals of Mn^{4+}, rather than Ni^{2+}. One would ask that, the distance of Mn-Mn is almost twice as much as C-C length, and what is the key factor to lead to the delocalization of Mn_6-ring to generate direct electronic exchange. Through electronic radial distribution for hydrogen-like atom, we note that rate of decay of *3d* electron is much slower than *2p* electron (Figure S7) to lead to more broad delocalization. The bond lengths of some good conductors, such as Cu and Au, are usually 2.56 ~ 2.95 Å, much larger than C-C length about 1.4 Å. So Mn-Mn length about 2.9 Å can be fitted to create the direct electronic delocalization interactions.

Magnetic coupling based on spin electrons not only benefits for direct interactions between Mn in Mn_6-ring but also facilitates interactions between TM and O elements. The superexchange interaction is a strong ferromagnetic (FM)/antiferromagnetic (AF) coupling between two next-to-nearest neighbor transition metals through a

nonmagnetic anion (Figure 5a and 5b).[26] The local Mn_6O_{24} clusters are connected by Ni through O. The superexchange interaction can lower the energy and consolidate the stability through ferrimagnetic configuration. The ELF plots of FM and AF configurations also show that AF configuration can further motivate the activation of O (Figure S8). Combined with previous reports,[27-28] compared with Mn^{4+}, the *d* band moves down in energy for Ni^{2+}. The filling of e'_g band increases, and the antibonding oxygen-metal *d* states become more populated and weaker. So Ni ions in the TM layer served as a median between Mn_6O_{24} clusters and don't need to bond so strongly as Mn-bonding in the cluster. But a stronger interaction is the interlayered 180° superexchange interaction that can strengthen the structure, as shown in Figure 5c. As mentioned earlier, symmetry-breaking of the Mn_6O_{24} cluster resulted by antisite-Ni (Ni_{anti}) are energetically favorable, in which the Ni_{anti} can interact with Mn_6-ring to be similar to the ferrocene (Fe sandwiched between two aromatic rings). Our calculation shows that antiparallel spins of 180° Ni_{anti}^{2+}-O-Ni^{2+} (parallel spins of 180° Ni_{anti}^{2+}-O-Mn^{4+}) can lower the energy by about 0.36 eV via comparing with parallel spins (antiparallel spins), which enhances the correlation between Mn_6O_{24} cluster with the entire structure. Thus, the origin of aromaticity of Mn_6-ring is direct interactions between Mn with the magnetic coupling of spin electrons and superexchange interaction of Mn-O-Mn with (*d-p-d)*π-electron delocalization in the Mn_6O_{24} cluster of flower structure.

Experimental characterization on the existence of Mn_6-ring. Yoon et al. studied ordering in $Li[Ni_xMn_{(2-x)/3}Li_{(1-2x)/3}]O_2$ (x = 1/10, 1/3, 1/2) by carefully analyzing

concentrations of the different Li environments in the transition-metal layers obtained from NMR and predicted from three different models for Li/Mn/Ni ordering.[13] They found that random model can not explain the experimental concentration of Li environments (e.g., $Li(OMn)_6$, $Li(OMn)_5(ONi)$) from all samples and the agreement of honeycomb model is good for the sample with lower Ni content. At high Ni content, Mn ions preferentially occupy sites surrounding Li and most is $Li(OMn)_6$ containing no Ni, indicating the tendency for Ni and Li avoidance. Combined with first principles simulations, a long-range $2\sqrt{3}$-type structure model (flower-like structure) in $Li(Ni_{0.5}Mn_{0.5})O_2$ with 8.7% Li/Ni exchange has been established: six manganese ions preferentially occupy coordination first ring surrounding the central Li-ion in the transition-metal layers, while twelve nickel ions tend to form the second ring encircling the first-ring.[13-14] The sophisticated neutron diffraction experiments provide further evidence for this flower-like structure though it is far from perfect.[29] However, characterizing detailed cation ordering is not an easy thing for experiments. For most experiments, only average cation positions form an O_3-type of layered $LiCoO_2$ can be given for $Li(Ni_{0.5}Mn_{0.5})O_2$. Subsequently, using a joint cluster expansion and Monte Carlo (MC) simulation, Hinuma et al. found that the flower-like structure transforms from ground state zigzag-ordered structure without Li/Ni disorder undergoing an irreversible phase transition over 550°.[19] When over 620°, the flower-like structure undergoes a reversible phase transition and changes to more disordered honeycomb structure, indicating flower-like structure is a low-energy stable phase. Chernova et al. also studied magnetic properties of $Li(Ni_{0.5}Mn_{0.5})O_2$ and gave a good explanation for

experimental data by assuming an imperfect flower-like ordering.[25] Thus, experimental characterization of layered $Li(Ni_{0.5}Mn_{0.5})O_2$ supported the existence of Mn_6-ring.

Conclusion

In summary, using ab initio calculations, we identified an inorganic aromaticity of Mn_6-ring in layered $Li(Ni_{0.5}Mn_{0.5})O_2$ with Ni/Li mixing. The delocalized orbitals Mn-d_{z2} in Mn_6-ring show similar electronic behavior as benzene-p_z does. It is also found that the direct delocalized interactions combined with the super-exchange interactions between TMs play a great role in forming the local Mn_6-ring in layered TM compounds. The delocalized interactions may exist in other transition metal ring systems, and the new insight provides important factors on governing the local ordering with an inorganic aromaticity in TM compounds.

ASSOCIATED CONTENT

Supporting Information

Supplemental Material provides more details about first-principle calculations. This material is available free of charge via the Internet at http://pubs.acs.org.

AUTHOR INFORMATION

Corresponding Author

* Feng Pan, Email address: panfeng@pkusz.edu.cn

Author Contributions

†These authors contributed equally to this work.

ACKNOWLEDGMENT

This work was financially supported by National Materials Ge-nome Project (2016YFB0700600), the National Natural Science Foundation of China (No. 21603007 and 51672012), and Shenzhen Science and Technology Research Grant (No. JCYJ20150729111733470 and JCYJ20151015162256516).

References

(1) Kekulé, A. Sur la constitution des substances aromatiques. *Bulletin mensuel de la Société Chimique de Paris* **1865**, *3*, 98.

(2) Bleeke, J. R. Metallabenzenes. *Chem. Rev.* **2001**, *101,* 1205-1227.

(3) Nyulászi, L. Aromaticity of phosphorus heterocycles. *Chem. Rev.* **2001**, *101,* 1229-1246.

(4) Minkin, V. I.; Minyaev, R. M. Cyclic aromatic systems with hypervalent centers. *Chem. Rev.* **2001**, *101,* 1247-1265.

(5) Katritzky, A. R.; Jug, K.; Oniciu, D. C. Quantitative measures of aromaticity for Mono-, Bi-, and tricyclic penta- and hexaatomic heteroaromatic ring systems and their interrelationships. *Chem. Rev.* **2001**, *101,* 1421-1449.

(6) Boldyrev, A. I.; Wang, L. S. All-metal aromaticity and antiaromaticity. *Chem. Rev.* **2005**, *105,* 3716-3757.

(7) Xie, Y.; Schreiner, P. R.; Schaefer, H. F.; Li, X. W.; Robinson, G. H. Are cyclogallenes $[M_2(GaH)_3]$ (M = Li, N, K) aromatic? *J. Am. Chem. Soc.* **1996**, *118*, 10635-10639.

(8) Li, X. Observation of All-Metal Aromatic Molecules. *Science* **2001**, *291*, 859-861.

(9) Li, X.; Zhang, H. F.; Wang, L. S.; Kuznetsov, A. E.; Cannon, N. A.; Boldyrev, A. I. Experimental and theoretical observations of aromaticity in heterocyclic XAl^{3-} (X = Si, Ge, Sn, Pb) systems. *Angew. Chem. Int. Ed.* **2001**, *40*, 1867-1870.

(10) Zhai, H. J.; Wang, L. S.; Kuznetsov, A. E.; Boldyrev, A. I. Probing the electronic structure and aromaticity of pentapnictogen cluster anions Pn_{5-} (Pn = P, As, Sb, and Bi) using photoelectron spectroscopy and ab initio calculations. *J. Phys. Chem. A* **2002**, *106*, 5600-5606.

(11) Qin, Q.; Zhou, L.; Wang, Y.; Sang, R.; Xu, L. $[ZnBi_4]^{3-}$ pentagon in K_6ZnBi_5: Aromatic all-metal heterocycle. *Inorg. Chem.* **2014**, *53*, 1266-1268.

(12) Meng, Y. S.; Ceder, G.; Grey, C. P.; Yoon, W. S.; Jiang, M.; Breger, J.; Shao-Horn, Y. Cation ordering in layered O3 $Li[Ni_xLi_{1/3-2x/3}]Mn_{2/3-x/3}]O_2$ (0 <= x <= 1/2) compounds. *Chem. Mater.* **2005**, *17*, 2386-2394.

(13) Yoon, W.-S.; Iannopollo, S.; Grey, C. P.; Carlier, D.; Gorman, J.; Reed, J.; Ceder, G. Local Structure and Cation Ordering in O3 Lithium Nickel Manganese Oxides with Stoichiometry $Li[Ni_xMn_{(2-x)/3}Li_{(1-2x)/3}]O_2$. *Electrochem. Solid-State Lett.* **2004**, *7*, A167.

(14) Van der Ven, A.; Ceder, G. Ordering in $Lix(Ni_{0.5}Mn_{0.5})O_2$ and its relation to charge capacity and electrochemical behavior in rechargeable lithium batteries. *Electrochem. Commun.* **2004**, *6*, 1045-1050.

(15) Dixit, M.; Kosa, M.; Lavi, O. S.; Markovsky, B.; Aurbach, D.; Major, D. T. Thermodynamic and kinetic

studies of $LiNi_{0.5}Co_{0.2}Mn_{0.3}O_2$ as a positive electrode material for Li-ion batteries using first principles. *Phys. Chem. Chem. Phys.* **2016**, *18*, 6799-6812.

(16) Cahill, L. S.; Yin, S. C.; Samoson, A.; Heinmaa, I.; Nazar, L. F.; Goward, G. R. ^{6}Li NMR studies of cation disorder and transition metal ordering in $Li[Ni_{1/3}Mn_{1/3}Co_{1/3}]O_2$ using ultrafast magic angle spinning. *Chem. Mater.* **2005**, *17*, 6560-6566.

(17) Wei, Y.; Zheng, J.; Cui, S.; Song, X.; Su, Y.; Deng, W.; Wu, Z.; Wang, X.; Wang, W.; Rao, M., et al. Kinetics Tuning of Li-Ion Diffusion in Layered $Li(Ni_xMn_yCo_z)O_2$. *J. Am. Chem. Soc.* **2015**, *137*, 8364-8367.

(18) Zheng, J.; Liu, T.; Hu, Z.; Wei, Y.; Song, X.; Ren, Y.; Wang, W.; Rao, M.; Lin, Y.; Chen, Z., et al. Tuning of Thermal Stability in Layered $Li(Ni_xMn_yCo_z)O_2$. *J. Am. Chem. Soc.* **2016**, *138*, 13326-13334.

(19) Hinuma, Y.; Meng, Y. S.; Kang, K. S.; Ceder, G. Phase transitions in the $LiNi_{0.5}Mn_{0.5}O_2$ system with temperature. *Chem. Mater.* **2007**, *19*, 1790-1800.

(20) Dianat, A.; Seriani, N.; Bobeth, M.; Cuniberti, G. Effects of Al-doping on the properties of Li-Mn-Ni-O cathode materials for Li-ion batteries: an ab initio study. *J. Mater. Chem. A* **2013**, *1*, 9273-9280.

(21) Dudarev, S. L.; Botton, G. A.; Savrasov, S. Y.; Humphreys, C. J.; Sutton, A. P. Electron-energy-loss spectra and the structural stability of nickel oxide: An LSDA+U study. *Phys. Rev. B* **1998**, *57*, 1505-1509.

(22) Hwang, B. J.; Tsai, Y. W.; Carlier, D.; Ceder, G. A combined computational/experimental study on $LiNi_{1/3}Co_{1/3}Mn_{1/3}O_2$. *Chem. Mater.* **2003**, *15*, 3676-3682.

(23) Dresselhaus, M. S.; Dresselhaus, G.; Jorio, A. *Group Theory: Application to the Physics of Condensed Matter*. Springer Berlin Heidelberg, 2007.

(24) Cooper, D. L.; Gerratt, J.; Raimondi, M. The Electronic-Structure Of the Benzene Molecule. *Nature* **1986**, *323*, 699-701.

(25) Chemova, N. A.; Ma, M.; Xiao, J.; Whittingham, M. S.; Breger, J.; Grey, C. P. Layered $Li_xNi_yMn_yCo_{1-2y}O_2$ cathodes for lithium ion batteries: Understanding local structure via magnetic properties. *Chem. Mater.* **2007**, *19*, 4682-4693.

(26) Kramers, H. A. The interaction between the magnetogenic atoms in a paramagnetic crystal. *Physica* **1934**, *1*, 182-192.

(27) Sun, H.; Zhao, K. J. Electronic Structure and Comparative Properties of $LiNi_xMn_yCo_zO_2$ Cathode Materials. *J. Phys. Chem. C.* **2017**, *121*, 6002-6010.

(28) Xie, Y.; Saubanere, M.; Doublet, M. L. Requirements for reversible extra-capacity in Li-rich layered oxides for Li-ion batteries. *Energy Environ. Sci.* **2017**, *10*, 266-274.

(29) Bréger, J.; Dupré, N.; Chupas, P. J.; Lee, P. L.; Proffen, T.; Parise, J. B.; Grey, C. P. Short- and long-range order in the positive electrode material, $Li(NiMn)_{0.5}O_2$: A joint X-ray and neutron diffraction, pair distribution function analysis and NMR study. *J. Am. Chem. Soc.* **2005**, *127*, 7529-7537.

Figures and Tables

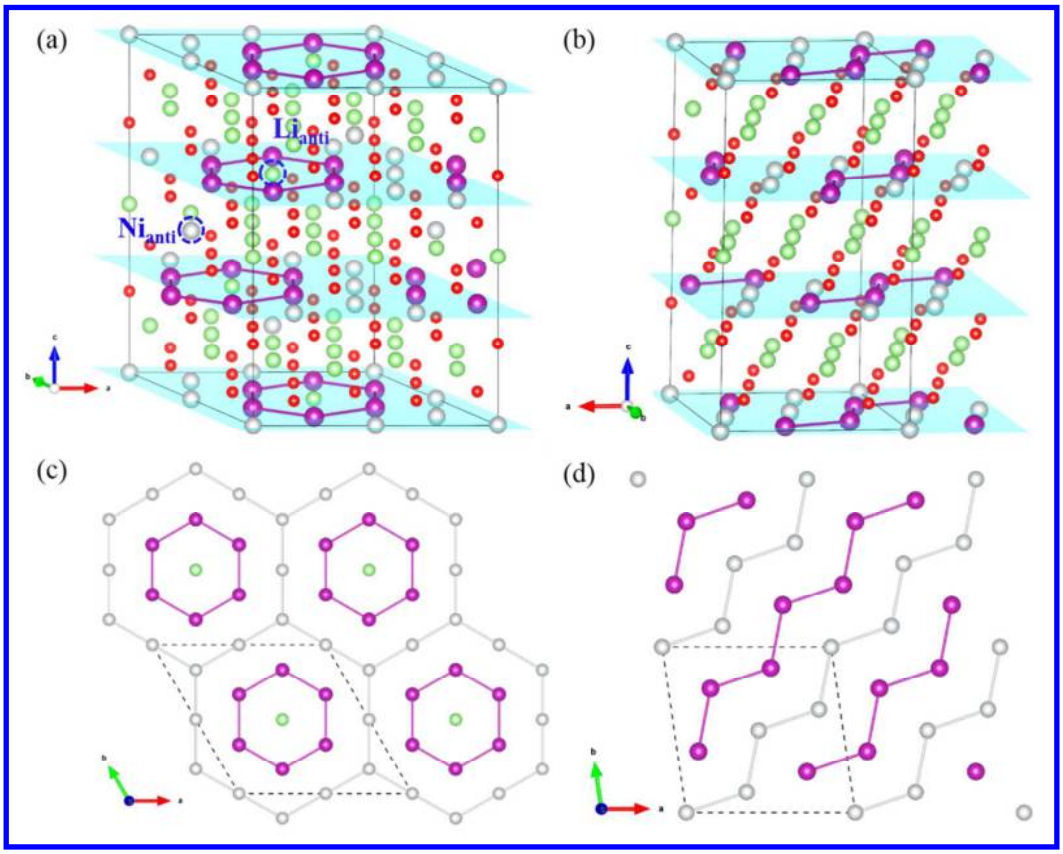

Figure 1. (a) The structure model of flower-like configuration with anti-Ni (Ni_a); (b) The structure model of zig-zag configuration; (c) The in-plane arrangement of TM in flower-like configuration; (d) The in-plane arrangements of TM in zig-zag

configuration. The purple, silvery, green and red spheres represent Mn, Ni, Li and O elements, respectively.

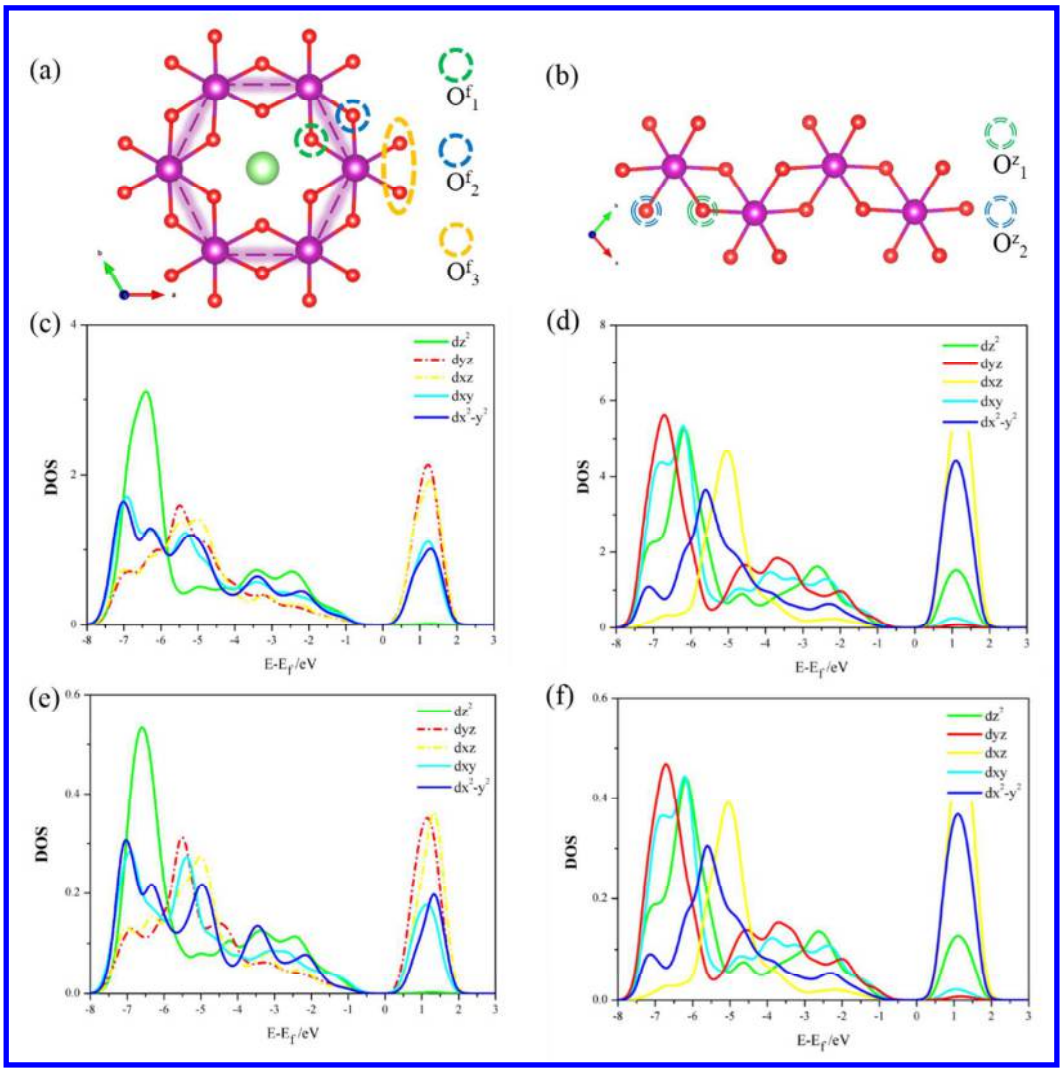

Figure 2. (a) The hypothetic Mn_6O_{24} cluster in flower-like configuration; (b) The structure fragment of Mn zig-zag chain. (c) The PDOS (projected density of states) of

flower-like configuration along the highest symmetry axis of the h-cluster; (d) The PDOS of zig-zag configuration along the highest symmetry axis of the MnO chain. (e) The PDOS of individual Mn in Mn_6-ring; (f) The PDOS of individual Mn in MnO chain.

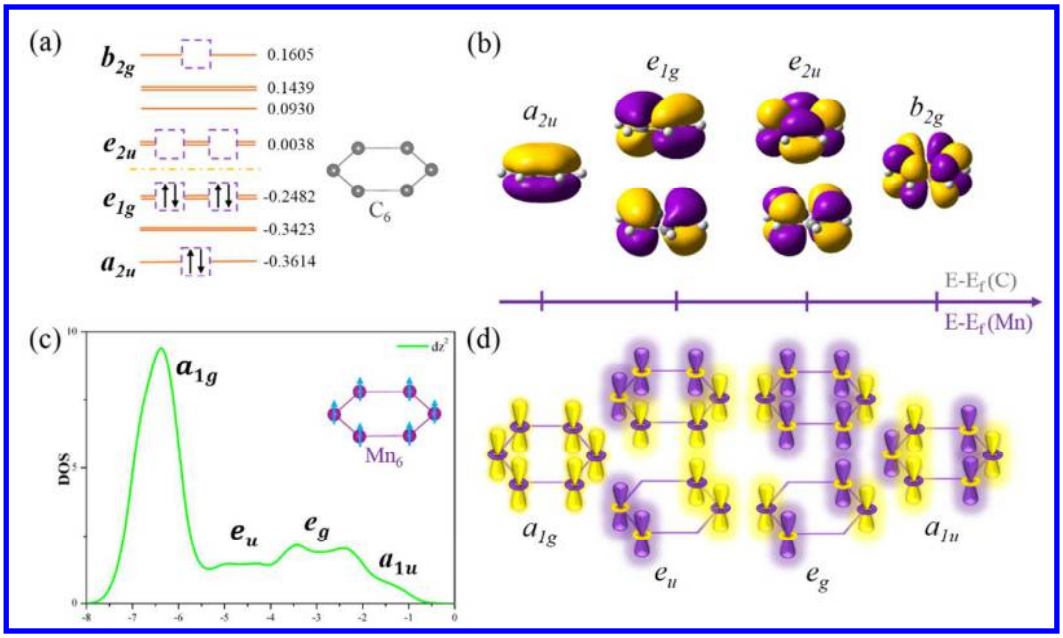

Figure 3. (a) The energy levels of C-p_z in benzene. (b) The delocalized orbitals of C-p_z, including two singlet-state (a_{2g}, b_{2u}) and two doublet-state (e_{1g}, e_{2u}). (c) The PDOS (projected density of states) of Mn-dz^2 orbitals in flower-like configuration. (d) The delocalized orbitals of Mn-dz^2 arranged in energy, including two singlet-state (a_{1g}, a_{1u}) and two doublet-state (e_u, e_g). The yellow parts of orbitals represent positive Wavefunction and the purple parts of orbitals represent negative Wavefunction.

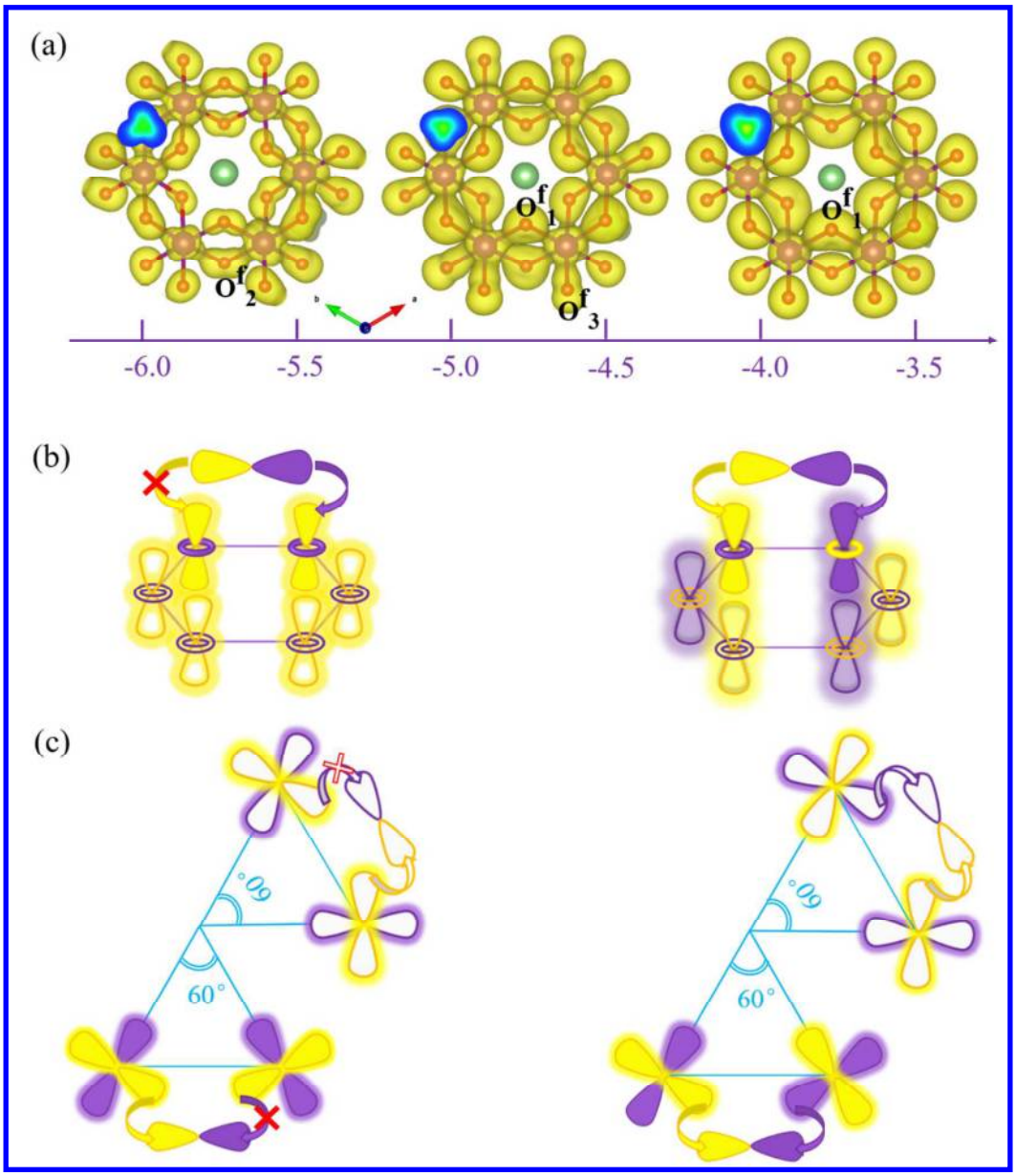

Figure 4. (a) The partials charge densities (PCD) arrange in energy from low to high. The varying patterns of PCD are restricted by O^f_1, O^f_2, O^f_3 groups. (b) The schematic

diagram interaction between delocalized d_{z2} of Mn_6-ring and O groups. (c) The schematic diagram interaction between delocalized d_{x2-y2} of Mn_6-ring and O groups. The yellow parts of orbitals represent positive Wavefunction, and the purple parts of orbitals represent negative Wavefunction.

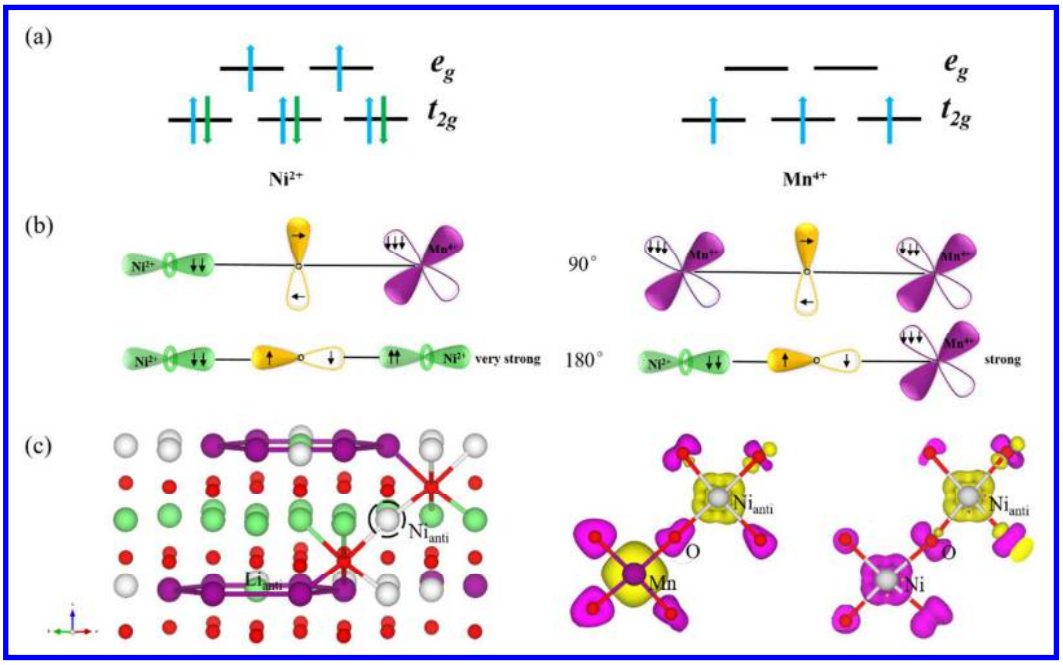

Figure 5. (a) Electronic configurations for TM ion in $Li(Ni_{1/2}Mn_{1/2})O_2$. (b) Schematic for 90˚ and 180˚ super-exchanges. (c) The interlayer 180° igusuperexchange interactions.

Table of Contents Synopsis: TM ions (here manganese) can interact with each other directly through delocalized orbitals in Mn_6-ring, and the local symmetry can impose restrictions on this delocalization. Degeneracy is inseparable nature of whole for Mn_6-ring due to entanglements between Mn cations.

Table of Contents Graphic